

Understanding the Specificity of a Docking Interaction between JNK1 and the Scaffolding Protein JIP1

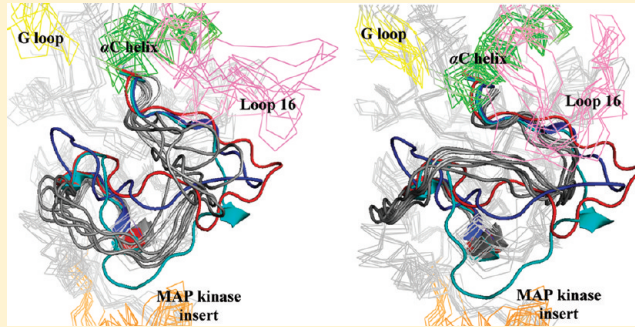
Chunli Yan,[†] Tamer Kaoud,[‡] Sunbae Lee,[‡] Kevin N. Dalby,^{*,‡,§} and Pengyu Ren^{*,†}

[†]Department of Biomedical Engineering, University of Texas, Austin, Texas 78712, United States

[‡]Division of Medicinal Chemistry, Graduate Program in Biochemistry and Molecular Biology and [§]Texas Institute for Drug and Diagnostic Development, University of Texas at Austin, Austin, Texas 78712, United States

 Supporting Information

ABSTRACT: The up-regulation of JNK activity is associated with a number of disease states. The JNK–JIP1 interaction represents an attractive target for the inhibition of JNK-mediated signaling. In this study, molecular dynamics simulations have been performed on the apo-JNK1 and the JNK1•L-pepJIP1 and JNK1•D-pepJIP1 complexes to investigate the interaction between the JIP1 peptides and JNK1. Dynamic domain studies based on essential dynamics (ED) analysis of apo-JNK1 and the JNK1•L-pepJIP1 complex have been performed to analyze and compare details of conformational changes, hinge axes, and hinge bending regions in both structures. The activation loop, the α C helix, and the G loop are found to be highly flexible and to exhibit significant changes in dynamics upon L-pepJIP1 binding. The conformation of the activation loop for the apo state is similar to that of inactive apo-ERK2, while the activation loop in JNK1•L-pepJIP1 complex resembles that of the inactive ERK2 bound with pepHePTP. ED analysis shows that, after the binding of L-pepJIP1, the N- and C-terminal domains of JNK1 display both a closure and a twisting motion centered around the activation loop, which functions as a hinge. In contrast, no domain motion is detected for the apo state for which an open conformation is favored. The present study suggests that L-pepJIP1 regulates the interdomain motions of JNK1 and potentially the active site via an allosteric mechanism. The binding free energies of L-pepJIP1 and D-pepJIP1 to JNK1 are estimated using the molecular mechanics Poisson–Boltzmann and generalized-Born surface area (MM-PB/GBSA) methods. The contribution of each residue at the interaction interface to the binding affinity of L-pepJIP1 with JNK1 has been analyzed by means of computational alanine-scanning mutagenesis and free energy decomposition. Several critical interactions for binding (e.g., Arg156/L-pepJIP1 and Glu329/JNK1) have been identified. The binding free energy calculation indicates that the electrostatic interaction contributes critically to specificity, rather than to binding affinity between the peptide and JNK1. Notably, the binding free energy calculations predict that D-pepJIP1 binding to JNK1 is significantly weaker than the L form, contradicting the previous suggestion that D-pepJIP1 acts as an inhibitor toward JNK1. We have performed experiments using purified JNK1 to confirm that, indeed, D-pepJIP1 does not inhibit the ability of JNK1 to phosphorylate c-Jun in vitro.



1. INTRODUCTION

Mitogen-activated protein (MAP) kinases play an essential role in the regulation of biological responses such as cell growth, oncogenic transformation, cell differentiation, apoptosis, and the immune response.^{1,2} The c-Jun N-terminal kinases (JNKs) belong to a subfamily of the MAP kinases and were first identified by their ability to phosphorylate the N-terminal transactivation domain of the transcription factor c-Jun.^{3–5} There are three JNK genes in mammals, Jnk1,³ Jnk2,⁴ and Jnk3,⁶ which produce at least 10 different isoforms of JNK through alternative splicing.^{6,7} JNK1 and JNK2 are ubiquitously expressed, while JNK3 is predominantly expressed in the heart, brain, and testis.^{6,8} The JNK isoforms share more than 90% amino acid sequence identity,

and the ATP-binding pocket is >98% homologous. These proteins are activated in response to various cytokines and cellular stresses such as heat shock, irradiation, hypoxia, chemo-toxins, and peroxides.^{1,2} Targets of the JNK signaling pathway include nuclear factor of activated T-cells (NFAT), activating transcription factor 2 (ATF2), E-26-like protein 1 (Elk1), c-Jun, and p53.^{9–11} Up-regulation of JNK activity is associated with a number of disease states such as type-2 diabetes, obesity, cancer, inflammation, and stroke.^{12–14} Therefore, JNK represents an

Received: August 5, 2010

Revised: December 7, 2010

Published: January 25, 2011

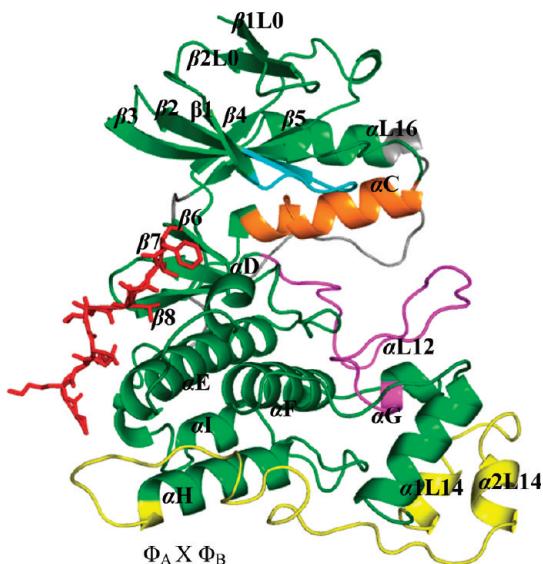


Figure 1. Cartoon diagram of the JNK1 structure highlighting the location of the L-pepJIP1 (red and sticks) (PDB ID: 1UKI)³⁰ and the sequences of the scaffolding protein (L-pepJIP1). The G loop is indicated in cyan, the MAP kinase insert in yellow, the α C helix in brown, the activation loop in magenta, the catalytic loop in blue, and the loop connecting the β 5 and β 6 and loop 16 in gray. The secondary structures are labeled based on ref 83.

attractive drug target for the development of novel therapeutic agents against a variety of diseases and has triggered extensive drug discovery efforts. Several ATP competitive JNK inhibitors have advanced into clinical trials.¹⁵

Scaffold proteins, known as JNK-interacting proteins or JIPs, contribute to the specificity and integrity of the JNK pathway. JNK-interacting protein-1 (JIP1), which was identified in a yeast two-hybrid analysis,¹⁵ is highly concentrated in the adult brain, being particularly enriched in the cerebral cortex and hippocampus.¹⁶ It contains a JNK-docking site that conforms to the well-described consensus sequence for a D-site, a sequence known to target the D-recruiting sites (DRSs) of MAPKs (Figure 1).¹⁷ This consensus sequence may be described as (R/K)_{2–3}-X_{1–6}- Φ_A - Φ_B , where Φ_A and Φ_B are hydrophobic residues, such as Leu, Ile, or Val. While the variability in the number and position of the hydrophobic and basic residues within the docking site contribute to specificity, these are not the only specificity determinants.^{18,19} The D-site of JIP1 is critical for the JNK-JIP1 interaction and the corresponding D-site peptide, L-pepJIP1 (amino acid sequence ¹⁵³RPKRPTTLNLF¹⁶³), inhibits JNK activity in vitro with remarkable selectivity exhibiting little inhibition of the related ERK and p38 MAPKs.^{16,20,21} Interestingly, it has been reported that a retro-inverso derivative of L-pepJIP1, synthesized from D-amino acids is a potent inhibitor of JNK1.^{20,21} Furthermore, this peptide, when fused to a cell-penetrating sequence, was reported to be more effective at preventing ROS-induced cell death than the parent peptide derived from L-amino acids.^{21,22}

Recent evidence suggests that interactions of the DRS of inactive MAPKs with D-site-containing ligands can induce various conformational changes within the MAPK activation loop of the catalytic domain with functional consequences. For example, Lim and Han showed that such interactions promote the autophosphorylation of a MAPK.^{23–26} When D-sites from MKK1,²⁷ He-PTP²⁷ and MKP3²⁸ are complexed to the DRS of

inactive ERK2, novel but stable conformations of the ERK2 activation loop are induced. In other cases, such as the binding of D-sites derived from MEF2A and MKK3B to the DRS of inactive p38 MAPK α , disorder is induced within the activation loop.²⁹ The first X-ray structure of inactive JNK1 in complex with L-pepJIP1 and the ATP-mimic SP600125 revealed an allosteric mechanism of binding.³⁰ Extensive rearrangements of the catalytic domain were reported to include a 15° interdomain rotation, closure of the active site cleft, distortion of the ATP-binding site, and a conformational transition from order to disorder in the activation loop.³⁰ A similar structural distortion of the ATP-binding site has been reported in the crystal structure of CDK6 bound to the tumor suppressor p16^{INK4a} or p19^{INK4d}.^{31,32}

The JNKs are regulated in a highly specific manner in cells, with a common feature being the binding of a D-site to the DRS of the JNK. Thus, binding of unactivated JNKs to MKKs or scaffolding proteins may involve interdomain rearrangements similar to those seen upon the formation of the JNK1•L-pepJIP1 complex. This inherent structural flexibility may play a central role in allowing the JNK pathway to be regulated by specific interactions with certain docking site proteins. Despite intense interest, many fundamental aspects of the JNK D-site/DRS interaction, such as the conformational change associated with L-pepJIP1 binding, the specificity of JNK1 for L-pepJIP1, and the selectivity of L-pepJIP1 for JNK over other MAPKs are not well understood.

Although crystallographic experiments provide critical time/ensemble-averaged structure and ligand binding information, atomic-level simulations yield additional insights and relevant biophysical information and have become increasingly important to understand complex conformational features of proteins and to predict structural preferences.^{33,34} An understanding of collective dynamics and correlations between different domains, or conformational states are vital for an understanding of protein function, because internal fluctuations and correlated dynamics of proteins intrinsically regulate their biological activities. Different computational approaches, such as molecular dynamics (MD), principle component analysis (PCA), and elastic network model have been applied to protein structures to investigate mechanisms of conformational switching.^{35–40} These methods work best for identifying global motions and geometrical differences. As no MD simulation study has been reported, to date, on the JIP1-induced domain closure of JNK1, we sought to apply this approach to gain new insights into how the fluctuations and long-range correlated motion induce the allosteric mechanism in different subdomains of JNK1. Also, given the apparent specificity of the L-pepJIP1 sequence for JNK1, it was of interest to compare the affinities of D-pepJIP1 and L-pepJIP1 for JNK1. Thus, a combination of explicit-solvent MD simulations, MM-PBSA/GBSA free energy calculations, and experimental assays were used to gain a deeper understanding of the structural and dynamical basis for allostery within the JNK1 polypeptide. The MM-PBSA method is an efficient way to evaluate the binding energetics from a classic MD simulation in explicit water. It has been applied to many different systems, including other protein recognition domains (e.g., the SH3 domains), and the relative affinities derived from the method have been compared successfully to experimental values.^{41–47} A variant of this method, termed MM-GBSA, in which the implicit generalized Born (GB) solvent model replaces the PB calculation, also exists.⁴⁸ Here we show that the binding of D-site peptide is highly coupled to the interdomain motion of JNK1 via an allosteric mechanism.

The MM-PBSA method is able to discriminate between the binding of mutant and wild type complexes. Computational alanine-scanning methodology was also performed to identify the important contributions to the overall protein–ligand binding.^{49–51}

2. COMPUTATIONAL AND EXPERIMENTAL DETAILS

2.1. Molecular Dynamics Simulation. The crystal structure of the L-pepJIP1 complexed with JNK1 was obtained from the RCSB Protein Data Bank (PDB ID: 1UKH).³⁰ The coordinates of the missing residues of JNK1 (Ala173–Arg189, Ala282–His286 and Ile337–His369) were added by using the homology software Modeller9v5.⁵² The apo form of JNK1 was then obtained by deleting L-pepJIP1 from the crystal structure. Mutations at specific residues of JNK1 (Arg127 and Glu329) were performed by using the LEaP module in the AMBER 9 software package⁵³ with the original crystal structure as the template.³⁰ D-pepJIP1 was modeled onto JNK1 according to the backbone atomic coordinates of L-pepJIP1 in the crystal complex. Molecular structure visualization and analysis were performed with PyMOL and VMD.^{54,55}

The LEaP module of AMBER 9 was used to add the missing hydrogen atoms of the proteins and to set all ionizable side chains to their characteristic ionization states at pH 7.0. Each system was solvated in a TIP3P water box with a minimum distance of 10.0 Å from the protein surface to the edge of the simulation box⁵⁶ followed by neutralization of each system by the counterions using the LEaP module. Minimizations and MD simulations were carried out using the Sander module of AMBER 9.⁵³ The AMBER ff03 force field was used for proteins and ions.⁵⁷ The particle mesh Ewald (PME) method was used to treat the long-range electrostatic interactions.⁵⁸ The cutoff distances for the real-space of the long-range electrostatic and the van der Waals interactions were set to 10.0 Å. All covalent bonds involving hydrogen atoms were constrained using the SHAKE algorithm.⁵⁹ Structure optimization was achieved in a stepwise manner with protein and ligand atoms initially fixed and the whole system then allowed to fully relax. In each step, energy minimization was executed using the steepest descent method for the first 2500 steps and then the conjugated gradient method for the subsequent 2500 steps. With a 0.05 ns molecular dynamics, the system was heated to 300 K. After a 0.05 ns NVT dynamics equilibration with weak positional restraints on the protein, 50.0 ns NPT dynamics simulation was performed for JNK1•L-pepJIP1, JNK1•D-pepJIP1, JNK1(R127A)•L-pepJIP1, JNK1(E329A)•L-pepJIP1, and 100 ns for the apo JNK1. An integration time step of 2.0 fs was used. The temperature was maintained at 300 K, and pressure was controlled at 1 atm using the Berendsen weak-coupling algorithm.⁶⁰ Atom coordinates were collected at an interval of 1.0 ps.

2.2. Binding Free Energy Calculation. The relative free energy of binding for peptide ligands, L-pepJIP1, and D-pepJIP1, to JNK1 was estimated by using the molecular mechanics Poisson–Boltzmann surface area (MM-PBSA) method^{41–47} in AMBER 9. The binding free energy for JNK1•L-pepJIP1, JNK1•D-pepJIP1, JNK1(R127A)•L-pepJIP1, and JNK1(E329A)•L-pepJIP1 was calculated as the average over the last 40 ns (1000 frames) from the trajectories. The free energy of binding was calculated for each snapshot using the following equation:

$$\Delta G_b = \Delta E_{MM} + \Delta G_{sol} - T\Delta S \quad (1)$$

where ΔE_{MM} is the gas-phase molecular mechanics binding energy, comprised of van der Waals and electrostatic contributions; ΔG_{sol} is the change in solvation free energy upon binding, consisting of

electrostatic and nonpolar interactions. The last term is the gas-phase entropy of change upon binding. The electrostatic solvation energy is determined using the finite difference Poisson–Boltzmann (PB) method or the generalized Born (GB) model.⁶¹ In the PB calculation, a 0.5 Å grid size was used, and the dielectric constants of protein and water were set to 1.0 and 80.0, respectively. The nonpolar contribution to the solvation free energy was determined from the solvent-accessible surface-area:

$$\Delta G_{nonpolar} = \gamma A + b \quad (2)$$

where A is the solvent-accessible surface area, and the solvation parameters γ and b are 0.0072 kcal mol⁻¹ Å⁻² and 0 kcal mol⁻¹, respectively. The probe radius of the solvent was set to 1.4 Å. The surface area A was calculated using the Molsurf in AMBER 9. The optimized atomic radii set in AMBER 9 were used, and the atomic charges of the protein were taken from the ff03 force field.⁵⁷ As the estimation of the entropic effect from normal-mode analysis is computationally very demanding, the entropy contribution was not included in this study. The interpretation will focus only on the relative values of the binding free energy, where the entropy contribution likely cancels for similar ligands.⁶²

2.3. Computational Alanine-Scanning Mutagenesis and Inhibitor-Residue Interaction Decomposition. The interaction between the ligand and JNK1 was further evaluated to assess the effect of substituting each residue for alanine (except glycine and proline) in the JNK/L-pepJIP1 interface. The binding free energy difference between the mutant and wild-type complexes is defined as

$$\Delta\Delta G_b = \Delta G_{mut} - \Delta G_{wt} \quad (3)$$

The interaction energies were further decomposed into contributions from JNK1 and ligand residue pairs. Moreover, contributions from JNK1 main chains and side chains were separated. The binding energy of each residue pair includes three terms: van der Waals contribution (ΔE_{vdw}), electrostatic contribution (ΔE_{ele}), and solvation contribution (ΔG_{GBSA}). The same dynamics trajectories utilized in the MM-PBSA calculations were used.

2.4. Essential Dynamics (ED) and Domain Motion Analysis. PCA was performed based on the covariance matrix C , whose elements are defined as

$$C_{ij} = \langle (x_i - \langle x_i \rangle)(x_j - \langle x_j \rangle) \rangle \quad (i, j = 1, 2, 3, \dots, 3N) \quad (4)$$

where x_i is a Cartesian coordinate of the i th C^α atom, N is the number of the C^α atoms considered, and $\langle x_i \rangle$ represents the time average over all the configurations obtained in the simulation. The central hypothesis of this method is that only the motions along the eigenvectors with large eigenvalues are important for describing the functionally significant motions in the protein.^{63,64} These important fluctuations are also referred to as the “essential” dynamic space. ED analyses of MD trajectories were performed using the PTRAJ module of AMBER 9. Porcupine plots were used to show the correlation between the movement of C^α atoms and functionally important motion.^{65,66} In the porcupine plots, needles were drawn for all residues corresponding to the implied movement of the respective residues for a given eigenvector. The arrows were drawn from the lowest to highest projection for each eigenvector. The porcupine plots were constructed using the programs VMD and IED.⁶⁷ Domain motion analysis based on PCA analysis was performed with the

DynDom 1.5.⁶⁸ DynDom analyzes the conformational changes of a protein in terms of dynamic domains, hinge axes, and hinge bending regions.^{35–37,40} This program was performed in three consecutive steps, i.e. searching the dynamics domains, determining the interdomain screw axes, and finally determining the bending regions.

2.5. JNK Kinase Activity Assay. JNK kinase assays were conducted at 30 °C in kinase assay buffer (25 mM HEPES buffer-pH 7.5, 50 mM KCl, 0.1 mM EDTA, 0.1 mM EGTA, 2 mM DTT and 10 µg/mL BSA), containing 20 nM active JNK1α1, 2 µM GST-c-jun (1–221), 300 µM [γ -³²P] ATP (100–1000 cpm pmol⁻¹), 11 mM MgCl₂, and different concentrations of JIP peptide in a final volume of 70 µL. JNK kinase activity was assessed at different peptide concentrations by the measurement of initial rates. Rates were measured under conditions where the total product formation represented less than 10% of the initial substrate concentrations. The reaction was initiated by the addition of ATP. Ten microliter aliquots were taken from every reaction at set time points (0.5, 1, 1.5, 2, 4 min) and spotted to 2 × 2 cm² of P81 cellulose paper; the papers were washed for 3 × 15 min in 50 mM phosphoric acid (H₃PO₄), then acetone, and then dried. The amount of labeled protein was determined by counting the associated cpm on a Packard 1500 scintillation counter at a σ value of 2.

3. RESULTS AND DISCUSSION

3.1. Structure and Dynamics of JNK1 from MD Simulation.

The structural organization of JNK1 is reported in Figure 1 and hereafter briefly summarized. The overall structure of JNK1 protein chains is essentially the same as observed for JNK3 (84% sequence identity, PDB ID: 1JNK)⁶⁹ and JNK2 (80% sequence identity, PDB ID: 3E7O).⁷⁰ JNK1 exhibits the classical bilobal kinase fold, where the N-terminal domain (N-lobe) is composed mainly of seven β -sheets (β 1L0, β 2L0, β 1, β 2, β 3, β 4 and β 5) and two α -helices (α L16 and α C) (Figure 1). The C-terminal domain (C-lobe) is predominantly α -helical and is linked to the N-terminus by two flexible loops. One loop (residues 108–112, following the JNK1 numbering) is located between β 5 and β 6, and the other (residues 331–351) connects α L16 to α I. The first loop partially defines the binding site for ATP and ATP-competitive kinase inhibitors. The second loop (loop 16) is the putative site of dimerization in active ERK2. The ceiling of the ATP-binding site, named the Gly-rich loop (G loop, residues 33–40), is rich in glycines. The activation loop (phosphorylation lip, residues 169–195), which connects the two terminal lobes belongs to the activation segment containing the phosphorylation sites, Thr183 and Tyr185. The activation loop is a structurally well-characterized region that begins with the conserved DFG motif (residues 169–171). A common sequence insertion in the MAP kinases is called “MAP kinase insert” (residues 251–288).

The conformational dynamics of JNK1, with and without peptide ligand, was examined using MD. Starting with the crystal structure of JNK1•L-pepJIP1, explicit-solvent molecular dynamics simulations were performed for five systems: apo-JNK1, JNK1•L-pepJIP1, JNK1•D-pepJIP1, JNK1(R127A)•L-pepJIP1, and JNK1(E329A)•L-pepJIP1. Note that no crystal structure is available for the apo form of JNK1. MD simulations of the apo structure were initiated using the complex crystal structure with the peptide extracted. The root-mean-square deviations (RMSDs) of the trajectories from the crystal structure

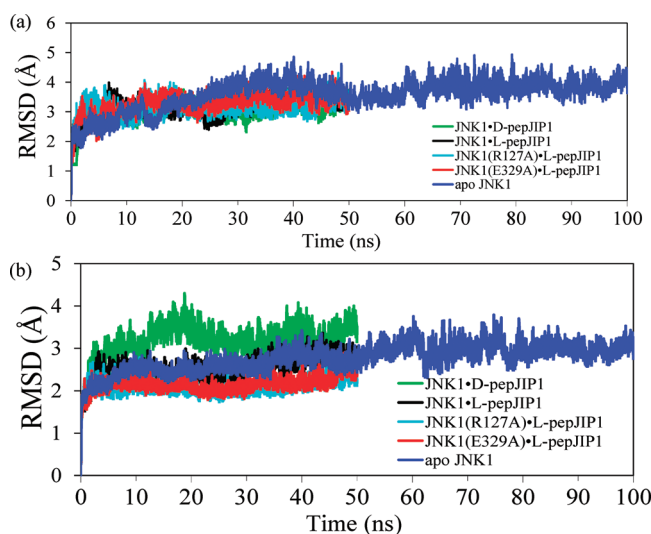


Figure 2. rmsd plots for the protein backbone of the complex formed between JNK1 and pepJIP1 relative to its initial structure: (a) with activation loop; (b) without activation loop.

were computed for (i) the entire protein (Figure 2a) and (ii) the entire protein excluding the activation loop (Figure 2b). Figure 2b reveals that the activation loop contributes to the major flexibility of the protein over the course of the simulation, as evidenced by the higher rmsd values when the contribution of the activation loop is included versus when it is excluded (i.e., 3 Å versus 2.0–2.5 Å). Thus, it appears that the activation loop causes an increased structural plasticity of JNK1. In contrast to complexes of L-pepJIP1, the calculated rmsd value of the JNK1•D-pepJIP1 complex is similar whether the activation loop is included in the calculation or not.

The rms fluctuation (rmsf) of the simulated structures about the crystal structure was calculated to characterize the regional motion in the protein structure. Figure 3 shows the atomic fluctuations averaged over residues for the five systems. Of the five systems studied, the apo-JNK1 has the largest fluctuations for all Ca, C, and N atoms. Overall, all five structures share similar rmsf profiles. The rmsf profiles indicate that the residues with higher fluctuation values are those in the glycine-rich loop (G loop, residues 33–40), the α C helix (residues 64–79), the activation loop region (residues 169–195), the MAP kinase insert (residues 251–288), and the protein termini. We shall note that a pronounced fluctuation of the activation loop and loop 16 can be observed in the apo JNK1. On the contrary, the binding of L-pepJIP1 to the DRS shows a lower mobility of the activation loop and loop 16. The observations reveal long-range conformational changes in the presence of D site peptide in JNK1. The activation loop in the JNK1•L-pepJIP1 X-ray crystal structures was found to be highly disordered.³⁰ Previously it was reported that the activation loop of p38 α MAP kinase became disordered upon binding of MEF2A or MKK3b peptide.²⁹ The activation loop of ERK2 was also found to display a new conformation upon peptide binding.²⁷ The DRS is formed by β 7– β 8 hairpin (residues 159–165), α D (residues 116–119, aa), and α E (residues 125–145) (Figure 1), which is distal from the ATP-binding pocket. This docking interaction has attracted pharmaceutical interest for the development of peptide-based therapeutic inhibitors and small molecule peptide mimics. As indicated by the rmsf plots (Figure 3), the DRS site exhibits a relatively smaller

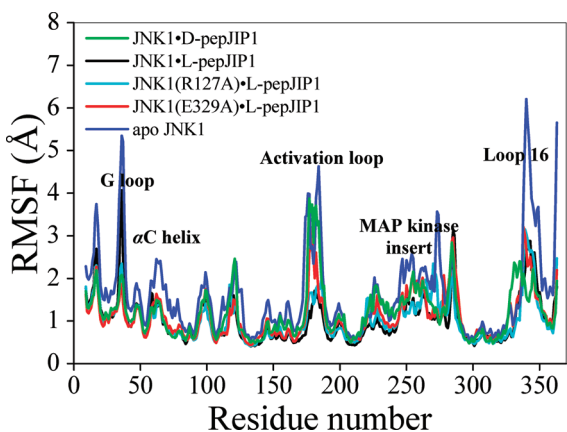


Figure 3. Atomic positional fluctuations of the C α , N, and C atoms of the systems.

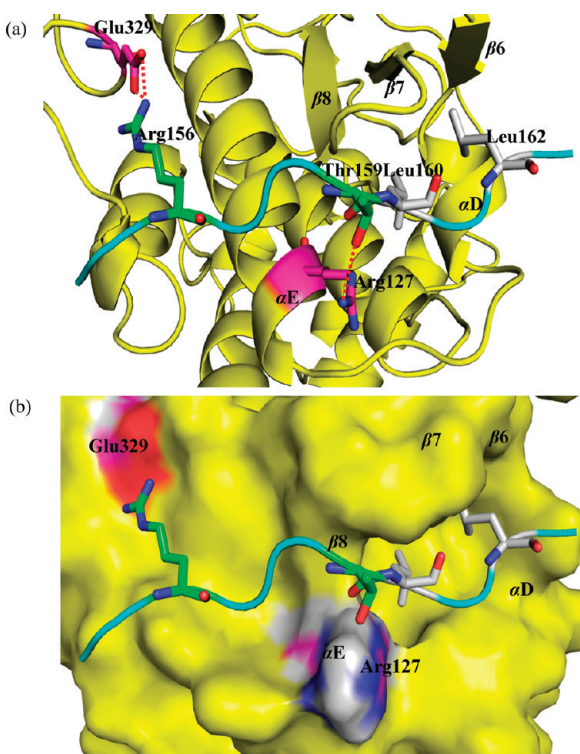


Figure 4. Stereo view of the binding specificity determining regions for L-pepJIP1 binding with JNK1. (a) Residues identified as critical in the alanine-scanning mutagenesis are shown in stick model. (b) Surface representation of JNK1 in complex with L-pepJIP1. Selected secondary structures are labeled. The dashed lines denote hydrogen bonds.

degree of conformational flexibility than some other regions of the protein.

Hydrogen bonds play an important role in molecular recognition. We examined 50 000 snapshots from the 50 ns trajectory to identify all direct hydrogen bonds. From the analysis, a few key interactions, mediated by long-lived hydrogen bonds between side-chain residues of JNK1 and L-pepJIP1, were identified (Table 1S, Supporting Information and Figure 4). The Arg156 side-chain of L-pepJIP1 makes two hydrogen bonds with the Glu329 side-chain of JNK1 (>90% occupied). The Thr159 side-chain of L-pepJIP1 forms one stable hydrogen bond with the Arg127 sidechain

of JNK1 (86% occupied). This result is consistent with the experimental finding that the replacement of Arg127 and Glu329 by alanine significantly reduced the binding affinity of L-pepJIP1 for JNK1.³⁰ The Arg127 and Glu329 of JNK1 are thus the key residues for L-pepJIP1 binding. On the other hand, no such hydrogen bonds between JNK1 and D-pepJIP1 were observed.

3.2. L-PepJIP1 Binding Induces Domain Motion. PCA enables isolation of the essential subspace from the local fluctuations via the calculation of a set of eigenvectors, which describe correlated motions of atoms within the MD simulation. To evaluate the dominant motion over an MD simulation, it is helpful to filter out all other motions by projecting the whole MD trajectory along the directions described by selected eigenvectors. The projections of a trajectory on the eigenvectors of its covariance matrix are called principal components. Through calculating the two extreme projections (minimum and maximum) on the time-averaged structure from the simulation, one can qualitatively understand the moving directions of each part of the protein. This method has proved to be an effective tool for investigating the motion tendencies of proteins from MD simulations.^{35–37,40}

Comparing the crystal structures of JNK3 with JNK1•L-pepJIP1, it was noted that the binding of pepJIP1 induced a hinge motion between the N- and C-terminal domains of JNK1.³⁰ To identify the systems' important modes of concerted motion, PCA analysis was performed using the 50 ns MD trajectories for the wild JNK1•L-pepJIP1 complex and the apo state. Out of the total 25 modes, the first three principal components account for approximately 62% and 64% of the variation for the JNK1•L-pepJIP1 complex and for the apo form, respectively (see Supporting Information). The porcupine plot of the first two modes in Figure 5a–d shows the amplitude of the motion undergone by each residue. In the JNK1•L-pepJIP1 complex, the most significant mode corresponds to the collective motion of the N-terminal domain relative to the C-terminal domain. Most of the movement in the two leading modes is concentrated in regions that also show the largest rms deviations (Figure 5), including the activation loop (blue), G-loop (green), αC helix (yellow) and loop 16 (ice blue). The G loop in the active site and the αC helix shows open/close motion with respect to the activation loop. The closer contacts between the C-terminal extension loop 16 and the activation loop in the JNK1•L-peptide complex promote tighter interactions between the two domains. Previous X-ray studies showed that, in ERK2, loop 16 is the main conformational linkage between the DRS site and the activation loop. The activation loop displays a new conformation.²⁷ An HX-MS analysis revealed that changes in backbone flexibility occur in the P+1 region upon peptide binding to the DRS.⁷¹ Moreover, the residues of these regions mainly move outward or inward from the active site. Such motions are relevant to the distortion of the ATP binding pocket.³⁰ We have compared the structures of the activation loop from our JNK1 simulation with the X-ray structures of the inactive form of apo ERK2,⁷² the inactive form of ERK2 in complex with pepHePTP,²⁷ and the active form of apo ERK2 (39% identical in amino acid sequence to JNK1) (Figure 6).⁷³ Interestingly, the conformation of the activation loop of the simulated apo JNK1 is very similar to that of the inactive form of apo ERK2.⁷² The activation loop of JNK1•L-peptide adopts a different conformation, which is, however, very similar to that of the inactive ERK2 bound with an inhibition peptide or active apo-ERK2, suggesting that the peptide binding induces a new conformation. Combining with the data on the

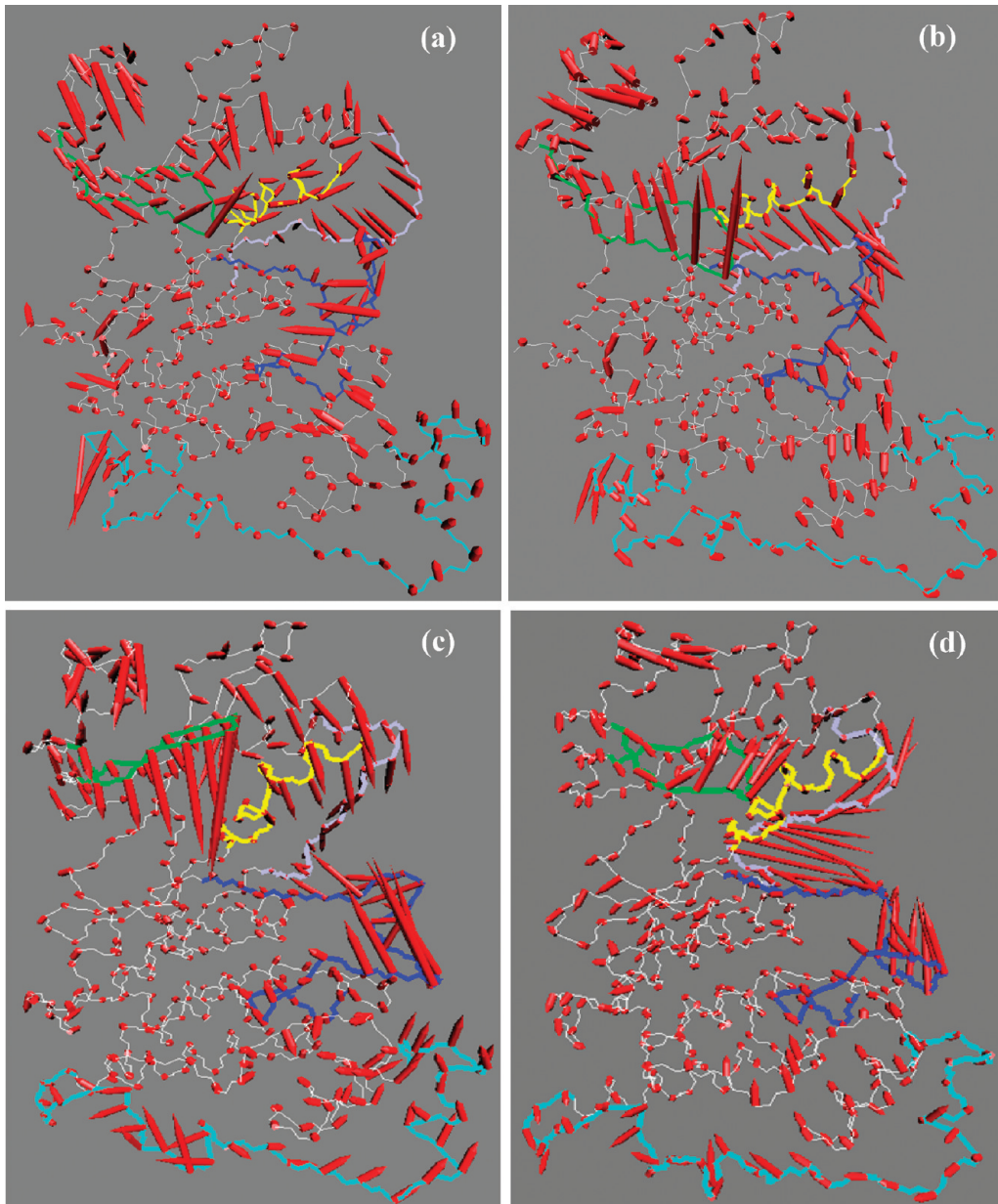


Figure 5. Porcupine plots of the two largest PCA modes from ED analysis of JNK1. The first and second motion modes for (a,b) the JNK1•L-pepJIP1 complex and (c,d) the apo-JNK1. Activation loop (blue), G loop (green), α C helix (yellow), loop 16 (ice blue), and MAP kinase insert (cyan). The arrows show mode.

rms fluctuation (Figure 3), the activation loop in the JNK1 complex shows less flexibility and higher rigidity than that of the apo-JNK1. Our observations suggest that the binding of the L-pepJIP1 to the DRS of JNK1 results in specific allosteric effects.

The effect of L-pepJIP1 on JNK1 dynamics becomes apparent when the relative movements of JNK1 domains in the complex are viewed as quasi-rigid bodies (Figure 7), based on the ED analysis via DynDom. Detailed output is given in the Supporting Information. Consistent with the PCA analysis, only the first and second modes of the JNK1 complex (Figure 7) were identified as related to domain motion, therefore representing the most significant fluctuations. The calculated inter domain screw-axes are shown as arrows in Figure 7 from the ED analysis. Figure 7a shows the domain motion of the JNK1 complex associated with the first eigenvector in terms of rotation of the region roughly

corresponding to the N-terminal domain (red) relative to the remaining JNK1 (C-terminal domain, blue). The moving domain (colored red in Figure 7a) composed of residues from the N-terminal domain rotates about 21.3° from the minimum to the maximum projection, with respect to the C-terminal domain. Both closure (67.3%) and twisting motions are displayed. The former refers to motion perpendicular to the hinge axis while the latter refers to motion parallel to the axis. The rigid-body motion seen here can potentially open up or narrow the entrance of the ATP binding pocket. This observation echoes previous work by Heo et al.,³⁰ which suggested that the distortion of the ATP-binding site was induced by the interdomain rearrangement upon L-pepJIP1 binding. This distortion may contribute to a significant reduction in the affinity of JNK for ATP affinity whose K_d increases 3-fold when L-pepJIP1 binds JNK1.³⁰ The bending

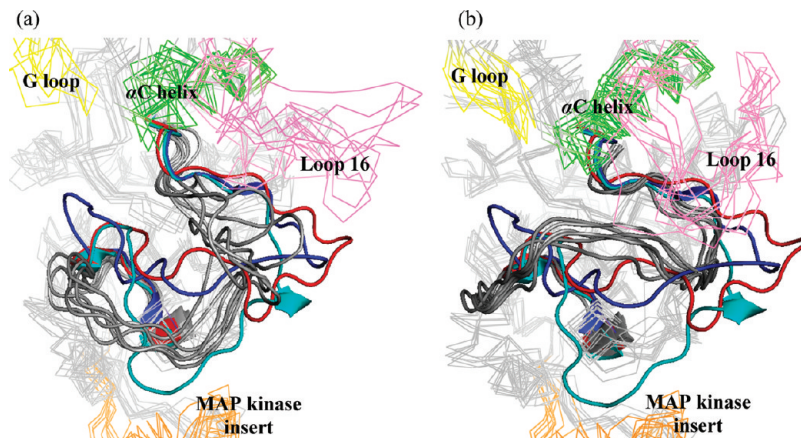


Figure 6. Stereoview superposition of the activation loop (gray) of JNK1 and ERK2. (a) apo-JNK1; (b) JNK1•L-pepJIP1. The inactive form of apo-ERK2 (cyan),⁷² the inactive form of ERK2 in complex with pepHePTP (blue),²⁷ and the active form (red) of ERK2.⁷³ The activation loops are shown in cartoon. Six snapshots are extracted from the last 40 ns trajectories randomly.

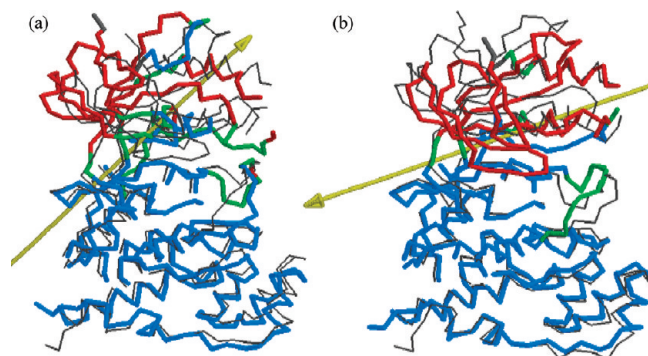


Figure 7. Dynamic domain identification of the JNK1•L-pepJIP1 complex for the first (a) and second (b) principal modes from the DynDom analysis. The arrows represent the hinge axes and the direction of rotation from conformer 1 to 2 (gray). The fixed domains are shown in blue, the residues involved in inter domain bending are green, and the moving domains are red.

regions (defined as the regions of the backbone that see a torsional transition) include residues 111–112 of the loop between $\beta 5$ and $\beta 6$, residues 331–334 of loop 16, and residues 174–179 and 181–182 of the activation loop. Figure 7b shows a rigid-body motion associated with the second eigenvector for the JNK1 complex. In this case, the motion is characterized by 87.0% closure, indicating that the interface between the C-terminal domain and N-terminal domain either widens or tightens upon rotation. The rotation from the minimum to maximum projection is about 26° . On the contrary, in the apo form of JNK1, the DynDom analysis performed on the three largest modes revealed none of the rigid-body domain motion as seen in the JNK1•L-pepJIP1 complex.

As a whole, JNK1 is characterized by an overall rigid body movement of domains that can be described as a combination of two orthogonal motions corresponding to movement of a large portion of the N-terminal domain relative to the C-terminal domain. The residues constituting the active site remain essentially rigid. We calculated the distance and angle between the center of mass of the two domains (C- and N-domains) during the simulation time, which is shown in Figure 8. It is clearly shown in Figure 8 that the distance between the center of mass of

the two domains in the apo state increased from 30 Å to 33 Å for the complex after the 30 ns simulation, and stabilized at 33 Å during the remaining simulations. The angle between domains opened up from $\sim 93^\circ$ to $\sim 104^\circ$ (Figure 8b). Thus JNK1 undergoes distinct structural changes and open conformation is favored upon removal of the peptide. Such conformational change is probably induced by peptide binding and may not happen in the apo structure. A previous study of Src and Lck kinases also pointed out that interlobe opening motion was necessary for the possible intramolecular self-activation.⁷⁴ There is unfortunately no crystal structure available for the apo structure. We have compared the MD simulated structures (apo and complex) with one existing X-ray structure of JNK1 with a small molecule inhibitor in the active site.⁷⁵ The simulated and experimental JNK1-pepJIP1 complex structures are very similar to that of JNK1 with inhibitor except in the activation loop region (overall rmsd: 1.5 Å).

3.3. Binding Interaction Energy. To analyze the energetics of L-pepJIP1 and D-pepJIP1 binding to JNK1, various components of the interaction free energy of the protein–peptide complexes were evaluated using an MM-PBSA analysis (Table 1). The estimated binding free energy ΔG_b for the wild type JNK1•L-pepJIP1 complex was significantly stronger than those for the JNK1 mutants. The binding free energies of JNK1(E329A)•L-pepJIP1 and JNK1(R127A)•L-pepJIP1 are weaker than those of JNK1•L-pepJIP1 by 8 kcal mol⁻¹ and 15 kcal mol⁻¹, respectively. The trend agrees with the experimental observation that the L-pepJIP1 binds to the mutants less favorably.³⁰ Biochemical data indicated that the K_d values for the binding of L-pepJIP1 to Glu329Ala and Arg127Ala increased by 22 times and 15 times, respectively, compared to wild JNK1.³⁰

Previous studies showed that a TAT fusion of D-pepJIP1 is more effective than the L counterpart in preventing ROS-induced cell death.^{21,22} Here we have computed the binding affinity of D-pepJIP1 to JNK1 and determine a calculated $\Delta \Delta G_b$ (D – L) of 26 kcal mol⁻¹, which suggests that D-pepJIP1 is a much weaker ligand for JNK1 than the L peptide. To verify this prediction, experiments were performed to evaluate the ability of L-pepJIP1 and D-pepJIP1 to inhibit the phosphorylation of c-Jun by JNK1 $\alpha 1$. As shown in Figure 9, L-pepJIP1 inhibits the JNK1-mediated phosphorylation of c-Jun in a dose-dependent manner with an IC_{50} of $1.0 \pm 0.1 \mu\text{M}$, which is consistent with a previous

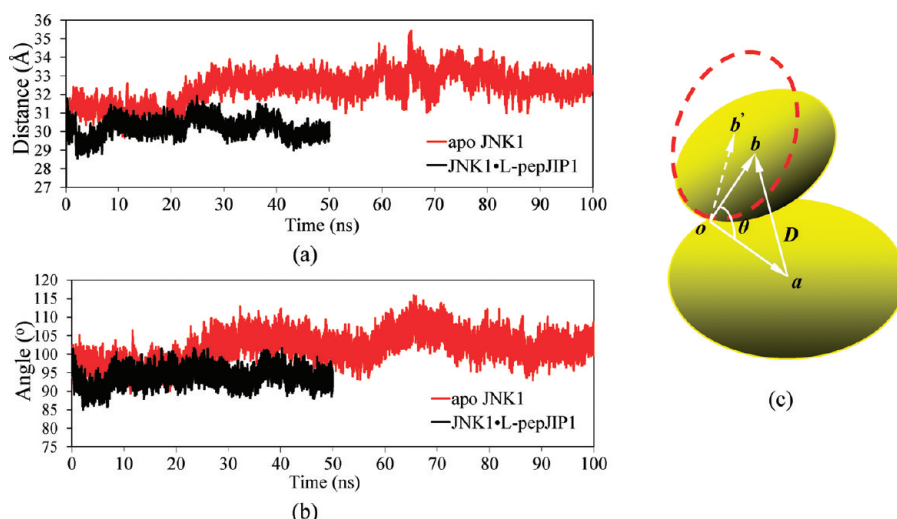


Figure 8. (a) Time evolution of the distance between the center of mass of the C- and N- domains of JNK1 during the production run. (b) Time evolution of the angle. (c) Definition of the distance (D) and angle (θ) for the N-terminal domain with respect to the C-terminal domain: The b and b' , the center of the N-terminal domain of the complex and apo JNK1; the o (reference point, CA of the hinge residue Met111); the a , the center of the C terminal domain of the complex and apo JNK1; θ , the angle between oa and ob (JNK1•L-pepJIP1) or ob' (apo).

Table 1. Free Energy Analysis (kcal mol⁻¹) for the Binding of PepJIP1 to JNK1

contribution	L-pepJIP1			
	JNK1	JNK1(R127A)	JNK1(E329A)	D-pepJIP1
ΔE_{ele}	-337.41 (24.22)	-368.26 (29.18)	-261.53 (37.19)	-160.03 (24.53)
ΔE_{vdw}	-64.66 (4.28)	-60.67 (4.54)	-66.49 (6.27)	-55.57 (6.80)
$\Delta G_{\text{nonpolar}}$	-9.87 (0.38)	-9.21 (0.46)	-9.65 (0.71)	-8.35 (0.82)
ΔG_{polar} (PB)	342.97 (22.42)	377.66 (28.21)	283.57 (38.99)	180.88 (24.63)
ΔG_{sol} (PB) ^a	333.11 (22.33)	368.45 (28.11)	273.92 (38.67)	172.53 (24.19)
ΔG_{ele} (PB) ^b	5.56 (5.72)	9.40 (6.21)	22.04 (9.11)	20.85 (7.87)
ΔG_{polar} (GB)	348.24 (22.79)	383.64 (28.18)	287.87 (37.40)	186.62 (24.47)
ΔG_{sol} (GB) ^a	338.37 (22.70)	374.43 (28.10)	278.22 (37.09)	178.27 (24.03)
ΔG_{ele} (GB) ^b	10.82 (4.63)	15.38 (4.08)	26.34 (6.26)	26.59 (5.96)
$\Delta\Delta G_b$ (PB/GB)	0	8.49/9.20	14.87/13.89	25.90/26.37
K_d (μM) ^c	0.42 ± 0	6.4 ± 2	9.1 ± 3	N/A
IC_{50} (μM) ^d	1.0 ± 0			

^aThe polar/nonpolar ($\Delta G_{\text{sol}} = \Delta G_{\text{polar}} + \Delta G_{\text{nonpolar}}$) contributions. ^bThe electrostatic ($\Delta G_{\text{ele}} = \Delta E_{\text{ele}} + \Delta G_{\text{polar}}$) contributions. ^cFrom ref 30. ^dFrom our work. Calculation of ΔG_b does not explicitly consider entropy contributions.

report by Heo et al.³⁰ who used isothermal titration calorimetry (ITC) to measure the binding of L-pepJIP1 to wild-type JNK1 and reported a K_d of $0.42 \pm 0.1 \mu\text{M}$. In contrast, D-pepJIP1 showed no ability to inhibit JNK1 at concentrations as high as $400 \mu\text{M}$ (Figure 10). These data indicate that D-pepJIP1 either does not bind to JNK1, or binds in such a configuration that it does not provide any inhibition. The free energy calculation suggests that it is likely to be the former.

We further analyzed the free energy components to search for the dominant interactions responsible for the observed binding specificity. According to the components of the binding free energies (Table 1), both the intermolecular (gas-phase) van der Waals and electrostatics interactions favor the binding. The electrostatic solvation (ΔG_{polar}) disfavors binding due to the cost associated with the desolvation of the peptide and JNK1 from the water environment. Nonpolar solvation, which corresponds to the burial of solvent-accessible surface area (SASA)

upon binding, gives a slightly favorable contribution. The total solvation energy, the sum of polar and nonpolar solvation terms, is unfavorable for all four complexes. The favorable contribution of the (gas-phase) electrostatic interactions between L-pepJIP1 and JNK1 is more than compensated for by the electrostatic desolvation free energy upon binding, so that the total electrostatic term (gas-phase and solvation combined) contributes somewhat unfavorably to the binding. It appears that for all four complexes the (gas-phase) van der Waals interactions contribute the most to the final binding free energy. It should be noted that the results do not suggest that electrostatic interactions are not important; on the contrary, electrostatic complementarity has to be satisfied for binding to occur. The electrostatic interaction essentially provides a negative selectivity filter that prevents binding of a nonspecific sequence. It seems common that MM/PB(GB)SA overestimates the absolute value of binding free energy likely due to the missing entropic contribution to

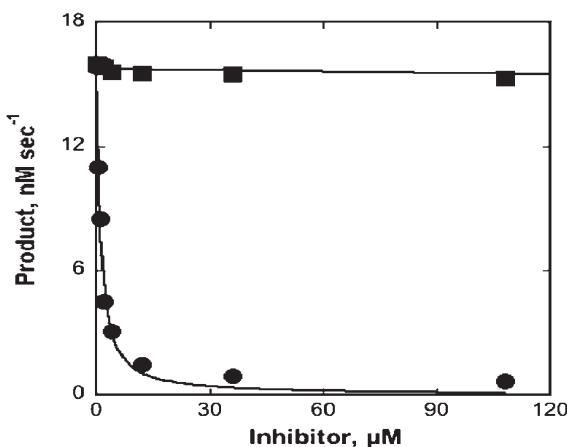


Figure 9. IC₅₀ Curves comparing the effect of L-pepJIP1 peptide (●) (a peptide corresponding to the D-domain of JIP1 scaffold protein-amino acids 153–163) and the D-pepJIP1 peptide (■) to inhibit JNK1α1 activity in vitro toward recombinant GST-C-JUN (1–221). L-pepJIP1 showed IC₅₀ of 1 ± 0.08 μM while D-pepJIP1 did not show any inhibition even at 400 μM.

binding.^{62,76–78} There is no good way of estimating binding entropy without running extensive simulations using alchemical or similar approaches. Even then it is unclear whether we can sample the peptide entropy reliably. Thus we did not calculate the entropic contribution in this work. On the other hand, the relative values of binding free energy could be more reliable due to error cancellation. The purpose of the free energy calculation here is to compare D- and L-peptide binding affinity to JNK1. The calculation essentially shows that the D-pepJIP1 has no affinity to JNK1 at the DRS site.

Binding free energy was decomposed into individual residue contributions at the interface of JNK1 and peptide as shown in Figure 10. This quantitative information is very useful for understanding the mechanistic basis for the formation of a protein–peptide complex. Molecular surface visualization and key residues for JNK inhibition are illustrated in Figure 4. The favorable residues are concentrated on a surface of the C-terminal domain of JNK1 and include Gln117 of αD, Arg127 and Tyr130 of αE, Glu329, and Trp324 (see Supporting Information, Table 3S). Glu329 and Arg127 form hydrogen bonds with Arg156 and Thr159 of L-pepJIP1, respectively. Based on the interaction spectrum in Figure 10, three residues in L-pepJIP1 (Arg156, Leu160, and Leu162) contribute dominantly to L-pepJIP1 binding. A previous experiment showed that Leu160 and Leu162 of the Φ_A-X-Φ_B motif in L-pepJIP1 form close contacts with the side chains of several hydrophobic residues (Ala113, Leu115, Val118, and Met121).³⁰ Asn161 of L-pepJIP1, the X residue in Φ_A-X-Φ_B motif, does not make a net contribution to binding, likely because it is compensated by a desolvation penalty. This result is consistent with the fact that the X residue has high diversity among MAPK ligands containing a docking site.^{79,80} The L-pepJIP1 terminal residues outside of the binding interface make little contribution to the binding.

3.4. Computational Mutagenesis of the Binding-Site Residues. Computational alanine scanning was performed to further elucidate the role of individual residues in the binding of L-pepJIP1 to JNK1. A total of 50 residues in JNK1 within 6 Å from the L-pepJIP1 and 8 residues of L-pepJIP1 (not including proline and glycine) were chosen for mutagenesis. Two different

approaches, PB and GB, were applied to evaluate the solvation component of the electrostatic free energies of solvation of protein and peptide. The computational mutagenesis was performed using the single-trajectory method,⁸¹ which has been shown to provide reasonable estimates for relative binding free energies.⁴⁹ The entropic contribution ($T\Delta S$) to the binding free energy was again not calculated in this study. In Figure 11a and b, we show the total binding free energy changes ($\Delta\Delta G_b$) upon mutation of each residue to alanine. The corresponding values of $\Delta\Delta G_b$, as well as the van der Waals ($\Delta\Delta E_{vdw}$), electrostatic ($\Delta\Delta E_{ele}$), and solvation components ($\Delta\Delta G_{polar}$), are given for each residue in the Supporting Information. In most cases, the change of electrostatic energy (gas-phase) and polar solvation free energies cancel. Therefore, we combined $\Delta\Delta E_{ele}$ and $\Delta\Delta G_{polar}$ together into $\Delta\Delta G_{ele}$.

Mutations of Arg127, Glu329, Trp324, and Tyr130 of JNK1 to alanine significantly reduced the free energy of binding L-pepJIP1 (Figure 11a), suggesting that these residues play an important role in the recognition. For L-pepJIP1, there are three residues—Arg156, Leu160, and Leu162—whose mutations lower the JNK1 affinity by more than 6 k_BT or 4 kcal mol⁻¹ (hotspots). The Glu329 (JNK1)-Arg156 (L-pepJIP1) interaction, which supports two hydrogen bonds (Figure 4), clearly represents the most dominant interacting pair. The Arg156Ala and Glu329Ala mutations reduced the binding free energy by 8 kcal mol⁻¹ and 15 kcal mol⁻¹, respectively. Most of the contribution, over 80%, arises from the electrostatic component (see Supporting Information). As we discussed earlier, while the salt–bridge pair does not seem to contribute significantly to the binding free energy of L-pepJIP1 to JNK1, mutation of either one would eliminate the binding specificity. In addition, the virtual alanine-scanning analysis suggests that Arg127 of JNK1 makes the second most dominant contribution (6 kcal mol⁻¹) to the binding. As shown in Figure 4, Arg127 forms a hydrogen bond with Thr159 of L-pepJIP1. Thus our calculations are in agreement with the experimental findings that the Arg127Ala and Glu329Ala mutations of JNK1 caused a significant reduction in its binding affinity for L-pepJIP1.³⁰ Leu160 and Leu162 of the Φ_A-X-Φ_B motif in L-pepJIP1 are surrounded by hydrophobic JNK1 residues, including Met121, Val118, Gln117, Leu115, Ala113, Leu123, Val59, and Leu131. According to the alanine-scanning, each L-pepJIP1 leucine is responsible for 7 kcal mol⁻¹ of binding free energy. Consistent with our computational alanine-scanning, Bogoyevitch et al. identified four residues (Arg156, Pro157, Leu160, or Leu162) as independently critical for JNK1 inhibition based on alanine replacement within truncated L-pepJIP1.²⁰

It has been suggested that the CD (common docking) domain, which is composed of acidic residues (e.g., Glu329 in the DRS of JNK1), is indispensable for the binding of most D-site ligands.⁸² However, X-ray crystallography was unable to identify a stable structure for the interaction between the acidic residues of p38 and the basic residues of the D-site peptides derived from ME-F2A or MKK3b.²⁹ Interestingly, our calculations indicate that the CD domain of JNK1 does not provide a favorable interaction with L-pepJIP1, rather it contributes to the specificity by penalizing an incorrect binding partner. This follows because the energy of attraction between the relevant ion-pairs is roughly equivalent to the combined free energy of desolvation of each charged residue. Thus, when one of the charged residues of an ion pair contributed by the CD domain (Glu329 of JNK1 and Arg156 of

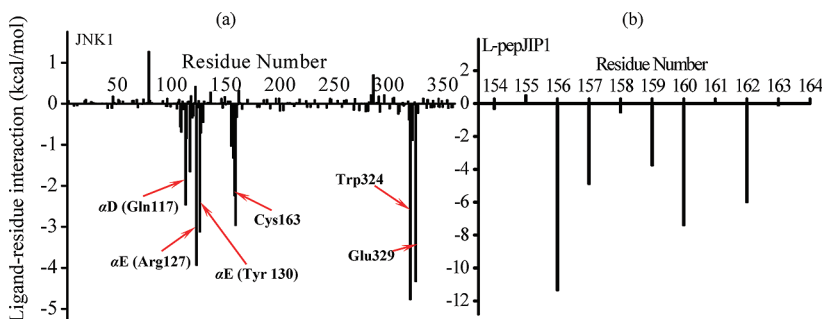


Figure 10. Ligand–residue interaction spectrum of (a) JNK1 and (b) L-pepJIP1.

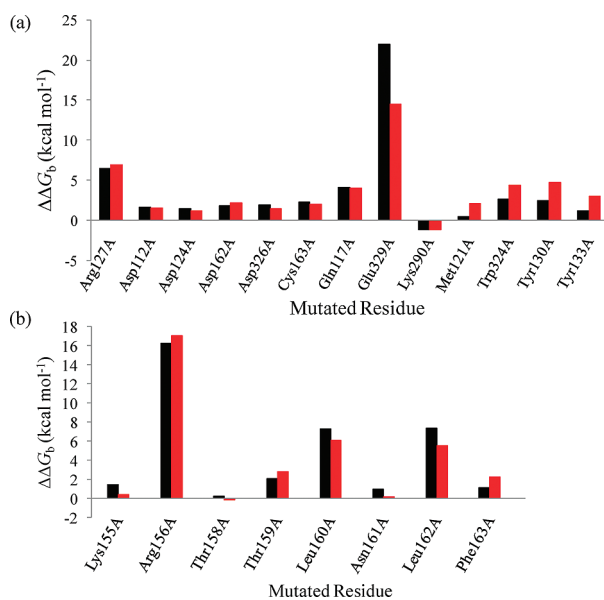


Figure 11. Comparison of $\Delta\Delta G_b$ values for L-pepJIP1 binding to JNK1 for alanine mutants. (a) JNK1; (b) L-pepJIP1. Relative binding free energy is the difference between binding free energy of wild-type JNK1 versus the alanine mutants: $\Delta\Delta G_b = \Delta G_b(\text{mut}) - \Delta G_b(\text{wild})$. Positive numbers in $\Delta\Delta G_b$ mean highly unfavorable substitutions. In contrast, negative $\Delta\Delta G_b$ indicates the preference for alanine mutation. The units of $\Delta\Delta G_b$ are kcal mol⁻¹. All values are provided in the Supporting Information.

L-pepJIP1) is mutated to Ala, it introduces a huge penalty because the desolvation of the cognate residue of the ion pair is no longer compensated by the appropriate gain in electrostatic attraction upon binding. Thus, the CD domain interaction may be viewed, to some degree, as providing a critical contribution to the specificity of the JNK1-L-pepJIP1 interaction, by essentially penalizing an incorrect binding partner.

The relative binding free energy $\Delta\Delta G_b$ calculated by the PB model are closely correlated with the values obtained by using the GB model for the 50 JNK1 and 8 L-pepJIP1 residues in the computational alanine scanning (correlation coefficient, $R^2 = 0.95$). We also compared the $\Delta\Delta G_b$ value obtained from the computational alanine-scanning with the free energy decomposition for the all 58 residues, with a R^2 of 0.90. Both methods highlight Arg127 and Glu329 of JNK1 and Arg156, Leu160, and Leu162 of L-pepJIP as important residues for the binding of L-pepJIP1 to JNK1. Overall, the results from the computational alanine scanning and free energy decomposition are consistent with each other. The current study will provide

useful guidelines to future experimental mutagenesis studies designed to increase the JNK1-JIP1 binding affinity and to discover new therapeutic agents targeting the JNK1-JIP1 interaction.

4. CONCLUSION

JNK1 (the c-Jun N-terminal kinase) plays a central role in linking obesity and insulin resistance. Docking interactions at the DRS of JNK are essential for JNK signaling. A small peptide derived from JIP1 is able to bind to the DRS of JNK and inhibit JNK activity in vitro. When fused to a cell penetrating sequence, it has been reported to inhibit JNK in mammalian cells.^{16,20,21} Furthermore, a retro-inverso form of the peptide fused to the TAT cell penetrating system has been reported to be effective in treating stroke in an animal model.^{20,21} These findings have stimulated the development of JNK inhibitors that target the DRS, rather than the highly conserved ATP binding site. Explicit-solvent MD simulations and ED analysis were performed to investigate the conformational dynamics within the apo-JNK1, JNK1•L-pepJIP1, and JNK1•D-pepJIP1 complexes. The ED-DynDom analysis of apo-JNK1 and the JNK1•L-pepJIP1 complex demonstrated a domain hinge-bending motion in the structures of the L-pepJIP1-bound. The conformation of the activation loop for the apo state differs from that of the JNK1•L-pepJIP1 complex and is similar to the inactive form of apo-ERK2 (Figure 6). Domain motion analysis suggests that L-pepJIP1 regulates the interdomain motion of JNK1 and the structure of the active site. In the apo JNK1 structure, the DynDom analysis does not reveal any rigid-body domain motion similar to that seen in the JNK1•L-pepJIP1 complex. The open conformation is favored for the apo form of JNK1, in agreement with the finding that the open conformation of Src and Lck kinase are needed for the possible autophosphorylation.⁷⁴ Using a continuum solvent model and generalized-Born model (MM-PB/GBSA), we have calculated the protein–peptide interaction energy. Computational alanine-scanning mutagenesis and free energy decomposition are performed to determine the contribution of each residue at the interaction interface to the binding of the peptide to JNK1. Interactions between the Arg156 of L-pepJIP1 with Glu329 of JNK1 and Thr159 of L-pepJIP1 with Arg127 of JNK1 have been identified as critical, in agreement with previous experiments. The electrostatic interaction at the CD domain does not make a significant contribution to the binding affinity between the peptide and JNK1 due to a significant desolvation penalty, but electrostatic complementarity is critical for selectivity as indicated by alanine scanning results. D-pepJIP1 peptide, a potent inhibitor of cell death, has been suggested to interact with JNK1 in a fashion similar to L-pepJIP1. However, our free energy

calculations show that the binding of D-pepJIP1 to JNK1 is much weaker (by 26 kcal mol⁻¹). This was confirmed by an absence of any observable inhibition of the phosphorylation of c-Jun by JNK1 in the presence of 400 μM D-pepJIP1. The present study provides valuable insight into the interactions and dynamics of JIP1 with JNK1. The results also serve as useful guidelines for future searches for high affinity/selectivity binding peptides and new therapeutic agents targeting the JNK1–JIP1 interactions.

■ ASSOCIATED CONTENT

§ Supporting Information. Full description of the experimental material (Construction of pET28a (+) Tev-JNK1α1, protein expression, and peptide synthesis), free energy data, DynDom output data, and PCA data. This material is available free of charge via the Internet at <http://pubs.acs.org>.

■ AUTHOR INFORMATION

Corresponding Author

*Phone: 512-232-1832. Fax: 512-232-1832. E-mail: pren@mail.utexas.edu (P.R.); dalby@mail.utexas.edu (K.N.D.).

■ ACKNOWLEDGMENT

Financial support for the computational studies was provided by the National Institute of General Medical Sciences (R01GM079686) and the Robert A. Welch Foundation (F-1691) to P.R. and by grants from the National Institute of General Medical Sciences (R01GM059802), the Welch Foundation (F-1390), and the Texas Institute for Drug & Diagnostic Development H-F-0032 to K.N.D. The authors gratefully acknowledge supercomputer time provided by the Texas Advanced Computing Center (TACC) and TeraGrid (MCB100057) at the University of Texas at Austin. The content is solely the responsibility of the authors and does not necessarily represent the official views of the National Institute of General Medical Sciences or the National Institutes of Health.

■ ABBREVIATIONS

JNK, c-Jun N-terminal kinase;
JIP1, JNK-interacting protein-1;
MAPK, mitogen-activated protein kinase;
DRS, D-recruiting site;
ERK, extracellular signal-regulated protein kinase;
MD, molecular dynamics;
PCA, principal component analysis;
ED, essential dynamics;
rmsd, root-mean-square deviation;
rmsf, root-mean-square fluctuation;
MM-PBSA/GBSA, molecular mechanics-Poisson–Boltzmann/generalized Born surface area;
ATP, adenosine triphosphate;
BSA, bovine serum albumin fraction V;
DTT, dithiothreitol;
EDTA, ethylene diamine tetraacetic acid;
EGTA, ethylene glycerol-bis[2-aminoethyl ether]-N,N,N',N'-tetraacetic acid;
HEPES, N-(2-hydroxyethyl)-piperazine-N'-2-ethanesulfonic acid;

IPTG, isopropyl-β-D-thiogalactopyranoside;
PCR, polymerase chain reaction;
ESI, electrospray ionization

■ REFERENCES

- (1) Kyriakis, J. M.; Avruch, J. *Physiol. Rev.* **2001**, *81*, 807–869.
- (2) Pearson, G.; Robinson, F.; Gibson, T. B.; Xu, B. E.; Karandikar, M.; Berman, K.; Cobb, M. H. *Endocr. Rev.* **2001**, *22*, 153–183.
- (3) Derijard, B.; Hibi, M.; Wu, I. H.; Barrett, T.; Su, B.; Deng, T. L.; Karin, M.; Davis, R. J. *J. Cell* **1994**, *76*, 1025–1037.
- (4) Kallunki, T.; Su, B.; Tsigleny, I.; Sluss, H. K.; Derijard, B.; Moore, G.; Davis, R.; Karin, M. *Genes Dev.* **1994**, *8*, 2996–3007.
- (5) Kyriakis, J. M.; Avruch, J. *J. Biol. Chem.* **1990**, *265*, 17355–17363.
- (6) Gupta, S.; Barrett, T.; Whitmarsh, A. J.; Cavanagh, J.; Sluss, H. K.; Derijard, B.; Davis, R. J. *EMBO J.* **1996**, *15*, 2760–2770.
- (7) Dreskin, S. C.; Thomas, G. W.; Dale, S. N.; Heasley, L. E. *J. Immunol.* **2001**, *166*, 5646–5653.
- (8) Martin, J. H.; Mohit, A. A.; Miller, C. A. *Mol. Brain Res.* **1996**, *35*, 47–57.
- (9) Gupta, S.; Campbell, D.; Derijard, B.; Davis, R. J. *Science* **1995**, *267*, 389–393.
- (10) Kraus, S.; Benard, O.; Naor, Z.; Seger, R. *J. Biol. Chem.* **2003**, *278*, 32618–32630.
- (11) Weston, C. R.; Davis, R. J. *Curr. Opin. Genet. Dev.* **2002**, *12*, 14–21.
- (12) Bogoyevitch, M. A. *Trends Mol. Med.* **2005**, *11*, 232–239.
- (13) Manning, A. M.; Davis, R. J. *Nat. Rev. Drug Discovery* **2003**, *2*, 554–565.
- (14) Manning, G.; Whyte, D. B.; Martinez, R.; Hunter, T.; Sudarsanam, S. *Science* **2002**, *298*, 1912–1934.
- (15) Whitmarsh, A. J.; Cavanagh, L.; Tournier, C.; Yasuda, L.; Davis, R. J. *Science* **1998**, *281*, 1671–1674.
- (16) Kim, I. J.; Lee, K. W.; Park, B. Y.; Lee, J. K.; Park, J.; Choi, I. Y.; Eom, S. J.; Chang, T. S.; Kim, M. J.; Yeom, Y. I.; Chang, S. K.; Lee, Y. D.; Choi, E. J.; Han, P. L. *J. Neurochem.* **1999**, *72*, 1335–1343.
- (17) Sharrocks, A. D.; Yang, S. H.; Galanis, A. *Trends Biochem. Sci.* **2000**, *25*, 448–453.
- (18) Smith, J. K.; Poteet-Smith, C. E.; Lannigan, D. A.; Freed, T. A.; Zoltoski, A. J.; Sturgill, T. W. *J. Biol. Chem.* **2000**, *275*, 31588–31593.
- (19) Tanoue, T.; Maeda, R.; Adachi, M.; Nishida, E. *EMBO J.* **2001**, *20*, 466–479.
- (20) Barr, R. K.; Kendrick, T. S.; Bogoyevitch, M. A. *J. Biol. Chem.* **2002**, *277*, 10987–10997.
- (21) Bonny, C.; Oberson, A.; Negri, S.; Sauser, C.; Schorderet, D. F. *Diabetes* **2001**, *50*, 77–82.
- (22) Milano, G.; Morel, S.; Bonny, C.; Samaja, M.; von Segesser, L. K.; Nicod, P.; Vassalli, G. *Am. J. Physiol. Heart Circ. Physiol.* **2007**, *292*, H1828–H1835.
- (23) Bhattacharyya, R. P.; Remenyi, A.; Good, M. C.; Bashor, C. J.; Falick, A. M.; Lim, W. A. *Science* **2006**, *311*, 822–826.
- (24) Ge, B. X.; Gram, H.; Di Padova, F.; Huang, B.; New, L.; Ulevitch, R. J.; Luo, Y.; Han, J. H. *Science* **2002**, *295*, 1291–1294.
- (25) Kang, Y. J.; Seit-Nebi, A.; Davis, R. J.; Han, J. H. *J. Biol. Chem.* **2006**, *281*, 26225–26234.
- (26) Remenyi, A.; Good, M. C.; Bhattacharyya, R. P.; Lim, W. A. *Mol. Cell* **2005**, *20*, 951–962.
- (27) Zhou, T.; Sun, L.; Humphreys, J.; Goldsmith, E. J. *Structure* **2006**, *14*, 1011–1019.
- (28) Liu, S.; Sun, J. P.; Zhou, B.; Zhang, Z. Y. *Proc. Natl. Acad. Sci. U.S.A.* **2006**, *103*, 5326–5331.
- (29) Chang, C. I.; Xu, B. E.; Akella, R.; Cobb, M. H.; Goldsmith, E. J. *Mol. Cell* **2002**, *9*, 1241–1249.
- (30) Heo, J. S.; Kim, S. K.; Seo, C. I.; Kim, Y. K.; Sung, B. J.; Lee, H. S.; Lee, J. I.; Park, S. Y.; Kim, J. H.; Hwang, K. Y.; Hyun, Y. L.; Jeon, Y. H.; Ro, S.; Cho, J. M.; Lee, T. G.; Yang, C. H. *EMBO J.* **2004**, *23*, 2185–2195.

- (31) Brotherton, D. H.; Dhanaraj, V.; Wick, S.; Brizuela, L.; Domaille, P. J.; Volyanik, E.; Xu, X.; Parisini, E.; Smith, B. O.; Archer, S. J.; Serrano, M.; Brenner, S. L.; Blundell, T. L.; Laue, E. D. *Nature* **1998**, *395*, 244–250.
- (32) Russo, A. A.; Tong, L.; Lee, J. O.; Jeffrey, P. D.; Pavletich, N. P. *Nature* **1998**, *395*, 237–243.
- (33) Simmerling, C.; Strockbine, B.; Roitberg, A. E. *J. Am. Chem. Soc.* **2002**, *124*, 11258–11259.
- (34) Snow, C. D.; Nguyen, N.; Pande, V. S.; Gruebele, M. *Nature* **2002**, *420*, 102–106.
- (35) Daidone, I.; Roccatano, D.; Hayward, S. *J. Mol. Biol.* **2004**, *339*, 515–525.
- (36) Hayward, S. *J. Mol. Biol.* **2004**, *339*, 1001–1021.
- (37) Hayward, S.; Kitao, A. *Biophys. J.* **2006**, *91*, 1823–1831.
- (38) Hyeon, C.; Jennings, P. A.; Adams, J. A.; Onuchic, J. N. *Proc. Natl. Acad. Sci. U.S.A.* **2009**, *106*, 3023–3028.
- (39) Liu, M. S.; Todd, B. D.; Sadus, R. J. *Aust. J. Chem.* **2010**, *63*, 405–412.
- (40) Roccatano, D.; Mark, A. E.; Hayward, S. *J. Mol. Biol.* **2001**, *310*, 1039–1053.
- (41) Bauer, F.; Schweimer, K.; Meiselbach, H.; Hoffmann, S.; Rosch, P.; Sticht, H. *Protein Sci.* **2005**, *14*, 2487–2498.
- (42) Gohlke, H.; Kiel, C.; Case, D. A. *J. Mol. Biol.* **2003**, *330*, 891–913.
- (43) Kollman, P. A.; Massova, I.; Reyes, C.; Kuhn, B.; Huo, S. H.; Chong, L.; Lee, M.; Lee, T.; Duan, Y.; Wang, W.; Donini, O.; Cieplak, P.; Srinivasan, J.; Case, D. A.; Cheatham, T. E. *Acc. Chem. Res.* **2000**, *33*, 889–897.
- (44) Kuhn, B.; Kollman, P. A. *J. Am. Chem. Soc.* **2000**, *122*, 3909–3916.
- (45) Massova, I.; Kollman, P. A. *Perspect. Drug Discovery Des.* **2000**, *18*, 113–135.
- (46) Masukawa, K. M.; Kollman, P. A.; Kuntz, I. D. *J. Med. Chem.* **2003**, *46*, 5628–5637.
- (47) Zhou, Z. G.; Madrid, M.; Evanseck, J. D.; Madura, J. D. *J. Am. Chem. Soc.* **2005**, *127*, 17253–17260.
- (48) Srinivasan, J.; Cheatham, T. E.; Cieplak, P.; Kollman, P. A.; Case, D. A. *J. Am. Chem. Soc.* **1998**, *120*, 9401–9409.
- (49) Lafont, V.; Schaefer, M.; Stote, R. H.; Altschuh, D.; Dejaegere, A. *Proteins: Struct., Funct., Bioinf.* **2007**, *67*, 418–434.
- (50) Moreira, I. S.; Fernandes, P. A.; Ramos, M. J. *J. Phys. Chem. B* **2006**, *110*, 10962–10969.
- (51) Moreira, I. S.; Fernandes, P. A.; Ramos, M. J. *J. Comput. Chem.* **2007**, *28*, 644–654.
- (52) Sanchez, R.; Sali, A. *Proteins: Struct., Funct., Genet.* **1997**, *Suppl. 1*, 50–58.
- (53) Case, D. A.; Cheatham, T. E.; Darden, T.; Gohlke, H.; Luo, R.; Merz, K. M.; Onufriev, A.; Simmerling, C.; Wang, B.; Woods, R. J. *J. Comput. Chem.* **2005**, *26*, 1668–1688.
- (54) Humphrey, W.; Dalke, A.; Schulter, K. *J. Mol. Graphics* **1996**, *14*, 33.
- (55) DeLano, W. L. *The PyMOL Molecular Graphics System*; DeLano Scientific: San Carlos, CA, 2002.
- (56) Jorgensen, W. L.; Chandrasekhar, J.; Madura, J. D.; Impey, R. W.; Klein, M. L. *J. Chem. Phys.* **1983**, *79*, 926–935.
- (57) Duan, Y.; Wu, C.; Chowdhury, S.; Lee, M. C.; Xiong, G. M.; Zhang, W.; Yang, R.; Cieplak, P.; Luo, R.; Lee, T.; Caldwell, J.; Wang, J. M.; Kollman, P. *J. Comput. Chem.* **2003**, *24*, 1999–2012.
- (58) Darden, T.; York, D.; Pedersen, L. *J. Chem. Phys.* **1993**, *98*, 10089–10092.
- (59) Ryckaert, J. P.; Ciccotti, G.; Berendsen, H. J. C. *J. Comput. Phys.* **1977**, *23*, 327–341.
- (60) Berendsen, H. J. C.; Postma, J. P. M.; Vangunsteren, W. F.; Dinola, A.; Haak, J. R. *J. Chem. Phys.* **1984**, *81*, 3684–3690.
- (61) Onufriev, A.; Bashford, D.; Case, D. A. *Proteins: Struct., Funct., Bioinf.* **2004**, *55*, 383–394.
- (62) Jiao, D.; Zhang, J. J.; Duke, R. E.; Li, G. H.; Schnieders, M. J.; Ren, P. Y. *J. Comput. Chem.* **2009**, *30*, 1701–1711.
- (63) Kitao, A.; Go, N. *Curr. Opin. Struct. Biol.* **1999**, *9*, 164–169.
- (64) Nolde, S. B.; Arseniev, A. S.; Orekhov, V. Y.; Billeter, M. *Proteins: Struct., Funct., Genet.* **2002**, *46*, 250–258.
- (65) Tai, K.; Shen, T. Y.; Borjesson, U.; Philippopoulos, M.; McCammon, J. A. *Biophys. J.* **2001**, *81*, 715–724.
- (66) Tai, K.; Shen, T. Y.; Henchman, R. H.; Bourne, Y.; Marchot, P.; McCammon, J. A. *J. Am. Chem. Soc.* **2002**, *124*, 6153–6161.
- (67) Mongan, J. *J. Comput.-Aided Mol. Des.* **2004**, *18*, 433–436.
- (68) Hayward, S.; Lee, R. A. *J. Mol. Graph. Model.* **2002**, *21*, 181–183.
- (69) Xie, X. L.; Gu, Y.; Fox, T.; Coll, J. T.; Fleming, M. A.; Markland, W.; Caron, P. R.; Wilson, K. P.; Su, M. S. S. *Structure* **1998**, *6*, 983–991.
- (70) Shaw, D.; Wang, S. M.; Villasenor, A. G.; Tsing, S.; Walter, D.; Browner, M. F.; Barnett, J.; Kuglstatter, A. *J. Mol. Biol.* **2008**, *383*, 885–893.
- (71) Lee, T.; Hoofnagle, A. N.; Kabuyama, Y.; Stroud, J.; Min, X. S.; Goldsmith, E. J.; Chen, L.; Resing, K. A.; Ahn, N. G. *Mol. Cell* **2004**, *14*, 43–55.
- (72) Zhang, F. M.; Strand, A.; Robbins, D.; Cobb, M. H.; Goldsmith, E. J. *Nature* **1994**, *367*, 704–711.
- (73) Canagarajah, B. J.; Khokhlatchev, A.; Cobb, M. H.; Goldsmith, E. J. *Cell* **1997**, *90*, 859–869.
- (74) Mendieta, J.; Gago, F. *J. Mol. Graph. Model.* **2004**, *23*, 189–198.
- (75) Chamberlain, S. D.; Redman, A. M.; Wilson, J. W.; Deanda, F.; Shotwell, J. B.; Gerding, R.; Lei, H. S.; Yang, B.; Stevens, K. L.; Hassell, A. M.; Shewchuk, L. M.; Leesnitzer, M. A.; Smith, J. L.; Sabbatini, P.; Atkins, C.; Groy, A.; Rowand, J. L.; Kumar, R.; Mook, R. A.; Moorthy, G.; Patnaik, S. *Bioorg. Med. Chem. Lett.* **2009**, *19*, 360–364.
- (76) Yan, C. L.; Xiu, Z. L.; Li, X. H.; Li, S. M.; Hao, C.; Teng, H. *Proteins: Struct., Funct., Bioinf.* **2008**, *73*, 134–149.
- (77) Zhu, X. L.; Hao, G.-F.; Zhan, C. G.; Yang, G. F. *J. Chem. Inf. Model.* **2009**, *49*, 1936–1943.
- (78) Zou, H. J.; Luo, C.; Zheng, S. X.; Luo, X. M.; Zhu, W. L.; Chen, K. X.; Shen, J. H.; Jiang, H. L. *J. Phys. Chem. B* **2007**, *111*, 9104–9113.
- (79) Holland, P. M.; Cooper, J. A. *Curr. Biol.* **1999**, *9*, R329–R331.
- (80) Yang, S. H.; Whitmarsh, A. J.; Davis, R. J.; Sharrocks, A. D. *EMBO J.* **1998**, *17*, 1740–1749.
- (81) Fogolari, F.; Brigo, A.; Molinari, H. *Biophys. J.* **2003**, *85*, 159–166.
- (82) Tanoue, T.; Nishida, E. *Pharmacol. Ther.* **2002**, *93*, 193–202.
- (83) Wang, Z. L.; Harkins, P. C.; Ulevitch, R. J.; Han, J. H.; Cobb, M. H.; Goldsmith, E. J. *Proc. Natl. Acad. Sci. U.S.A.* **1997**, *94*, 2327–2332.